JOURNAL OF MATERIALS SCIENCE 33 (1998) 2577–2582

Formation of the fluorite phase and other related phases in the system Y_2O_3–Ta_2O_5–MO (M=Mg, Ca, Sr or Ba)

SOON MOK CHOI, HONG LIM LEE
Department of Ceramic Engineering, Yonsei University, Seoul, 120-749, South Korea
E-mail: html1@bubble.yonsei.ac.kr

SHIN KIM
Fine Ceramics Division, Institute of Ceramic Technology, Seoul 153-023, South Korea

The formation of the fluorite phase $Y_{0.8}Ta_{0.2}O_{1.7}$ and other related phases in the system Y_2O_3–Ta_2O_5–MO (M = Mg, Ca, Sr or Ba) has been studied. The single fluorite phase formed when up to 12 mol% MgO was added to the fluorite phase; however, MgO appeared as the second phase as well as the main fluorite phase when more than 16 mol% MgO was added. When more than 8 mol% CaO was added to $Y_{0.8}Ta_{0.2}O_{1.7}$, Ca_2YTaO_6 and Y_2O_3 were produced as the second phases as well as the main fluorite phase. Ba_2YTaO_6 and Sr_2YTaO_6 of the perovskite-type ordered structure and Y_2O_3 were produced as well as the main fluorite phase when only 4 mol% BaO or SrO were added to $Y_{0.8}Ta_{0.2}O_{17}$. The region of the fluorite single phase was found in the system Y_2O_3–Ta_2O_5–CaO. The formation of the fluorite phase is assumed to be related to the cation radius of the doped alkaline-earth oxide.

1. Introduction

Fluorite-type oxides which are solid oxide ionic conductors are of interest for their applications to fuel cells, electrolysers and gas sensors [1, 2]. In this fluorite structure, cations are in eightfold coordination with their nearest neighbours, and each anion is surrounded tetrahedrally by four cations [3]. There are also many other oxides such as CeO_2, ThO_2 and UO_2 which have the fluorite structure. HfO_2 and ZrO_2 also retain the fluorite structure down to room temperature by the formation of solid solutions with divalent cationic oxides such as MgO and CaO or a trivalent cationic oxide such as Y_2O_3 [4, 5]. By doping the fluorite-type oxide with oxides whose cationic valencies are less than those of the host cations, oxygen-ion vacancies are produced, thereby achieving electrical neutrality in the substituted fluorite lattice [6]. This oxygen vacancy brings about the oxygen ionic conductivity at high temperatures.

The formation of the fluorite and other related structures in ternary systems has been reported in the systems ZrO_2–Y_2O_3–Ta_2O_5 [7, 8], ZrO_2–La_2O_3–Nb_2O_5 [9], HfO_2–Er_2O_3–Ta_2O_3 [10] and $ZrO_2(HfO_2)$–MgO–$Nb_2O_3(Ta_2O_5)$ [11]. Of the rare-earth oxide (R_2O_3)-alkaline-earth oxide (MO)–$Ta_2O_5(Nb_2O_5)$ ternary systems, only the system La_2O_3–SrO–Nb_2O_5 [12] has been studied but the formation of the fluorite phase has not been reported. The fluorite phase was reported to form in some binary systems containing Y_2O_3 or other rare-earth oxides [13–16]. The fluorite structure was reported to form in the system Y_2O_3–TiO_2 above about 1400 °C together with the main phase Y_2TiO_5 [13]. The fluorite related structure Lu_2TiO_5 was reported to form in the Lu_2O_3–TiO_2 system [14]. Recently, the fluorite structure was found to form with the composition $4R_2O_3{\cdot}Ta_2O_5$ ($R_{0.8}Ta_{0.2}O_{1.7}$) in rare-earth oxide–Ta_2O_5 systems above about 1700 °C [15, 16].

In this study the ternary systems of Y_2O_3–Ta_2O_5–MO (M = Mg, Ca, Sr or Ba), including the system $Y_{0.8}Ta_{0.2}O_{1.7}$–MO, were investigated to find the regions of the fluorite single phase and other related phases.

2. Experimental procedure

As the starting materials, Y_2O_3, Ta_2O_5, $BaCO_3$, $SrCO_3$, $CaCO_3$ and MgO were used. All materials were reagent grades and purer than 99.9%.

To obtain the fluorite phase $Y_{0.8}Ta_{0.2}O_{1.7}$ which is very important in the binary system Y_2O_3–Ta_2O_5, Y_2O_3 and Ta_2O_5 powders were mixed and milled in an alumina mortar with an Y^{3+}: Ta^{5+} molar ratio of 4:1. The mixed powder was pressed into discs before being heated at 1350 °C for 24 h in air. The heat-treated discs were crushed into powder and were mixed with MgO, $CaCO_3$, $SrCO_3$ or $BaCO_3$ powders, respectively, in various concentrations of 4–20 mol% of their oxide forms as shown in Table I and pressed into discs again. This process of heat treatment and

crushing was repeated twice for homogenization of the compositions of the final samples. The crushed powders were pressed into disc-type specimens and pressed isostatically under 20 000 lbf in^{-2}. The specimens were fired at 1650 °C for 5 h and cooled to room temperature at the rate of 10 °C min^{-1}.

To determine the phase relations around the fluorite phase $Y_{0.8}Ta_{0.2}O_{1.7}$ in the ternary system Y_2O_3–TaO–CaO at 1650 °C, the specimens were prepared in various compositions as shown in Table II using the same Y_2O_3, Ta_2O_5 and $CaCO_3$ powders and the same method as mentioned above until the final disc-type specimens were obtained by being pressed isostatically under 20 000 lbf in^{-2} and fired at 1650 °C for 5 h and cooled to room temperature at the rate of 10 °C min^{-1}.

The obtained specimens were analysed by the X-ray powder diffraction method to confirm the formation of fluorite and other related phases.

3. Results and discussion

The various compositions studied in the system Y_2O_3–Ta_2O_5–CaO are represented in Tables I and II and in Fig. 1. As shown in Fig. 1, the point A is located on the straight line drawn vertically from the composition with 77.5 mol% Y_2O_3 in the binary system Y_2O_3–Ta_2O_5 and the points B, C and D are located on the straight line drawn vertically from the composition with 75 mol% Y_2O_3 in the binary system Y_2O_3–Ta_2O_5. The compositions of the points E, F and G contain 4, 8 and 12 mol% CaO, respectively, keeping the molar ratio of the remaining compositions of Y_2O_3 and Ta_2O_5 to be constant with the Y_2O_3:Ta_2O_5 ratio of 75:25 as given in Table II.

Fig. 2 shows the X-ray diffraction patterns of the specimens in which the fluorite phase $Y_{0.8}Ta_{0.2}O_{1.7}$

TABLE I The compositions of the specimens studied in the system $Y_{0.8}Ta_{0.2}O_{1.7}$–MO

Specimen	MO (mol%)	$Y_{0.8}Ta_{0.2}O_{1.7}$ (mol%)
Mg4	4 MgO	96
Mg8	8 MgO	92
Mg12	12 MgO	88
Mg16	16 MgO	84
Mg20	20 MgO	80
Ca4	4 CaO	96
Ca8	8 CaO	92
Ca12	12 CaO	88
Sr4	4 SrO	96
Ba4	4 BaO	96

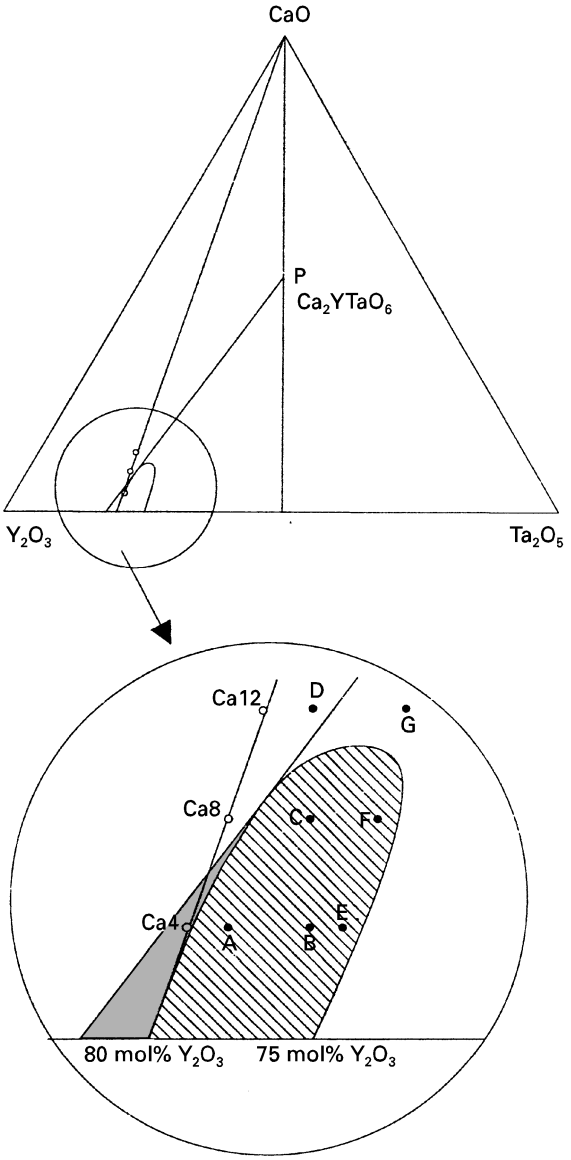

Figure 1 The compositions of the specimens studied in the ternary system Y_2O_3–Ta_2O_5–CaO.

TABLE II The compositions of the specimens studied in the system Y_2O_3–Ta_2O_5–CaO

Point in Fig. 1	CaO concentration (mol%)	Y_2O_3 concentration (mol%)	Ta_2O_5 concentration (mol%)	$[Y_2O_3]/[Y_2O_3]+[Ta_2O_5]$
A	4.0	75.5	20.5	0.7865
B	4.0	73.0	23.0	0.7604
C	8.0	71.7	20.3	0.7797
D	12.0	69.0	19.0	0.7841
E	4.0	72.0	24.0	0.75
F	8.0	69.0	23.0	0.75
G	12.0	66.0	22.0	0.75

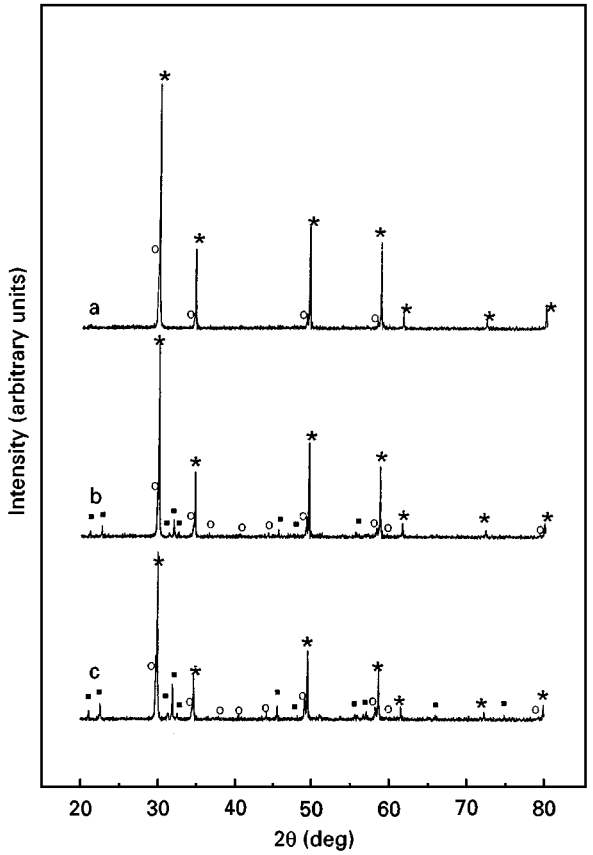

Figure 2 X-ray diffraction patterns of the fluorite $Y_{0.8}Ta_{0.2}O_{1.7}$ specimens doped with 4 mol% CaO (specimen Ca4) (curve a), 8 mol% CaO (specimen Ca8) (curve b) and 12 mol% CaO (specimen Ca12) (curve c). (*), fluorite; (○), cubic Y_2O_3; (■), monoclinic Ca_2YTaO_6.

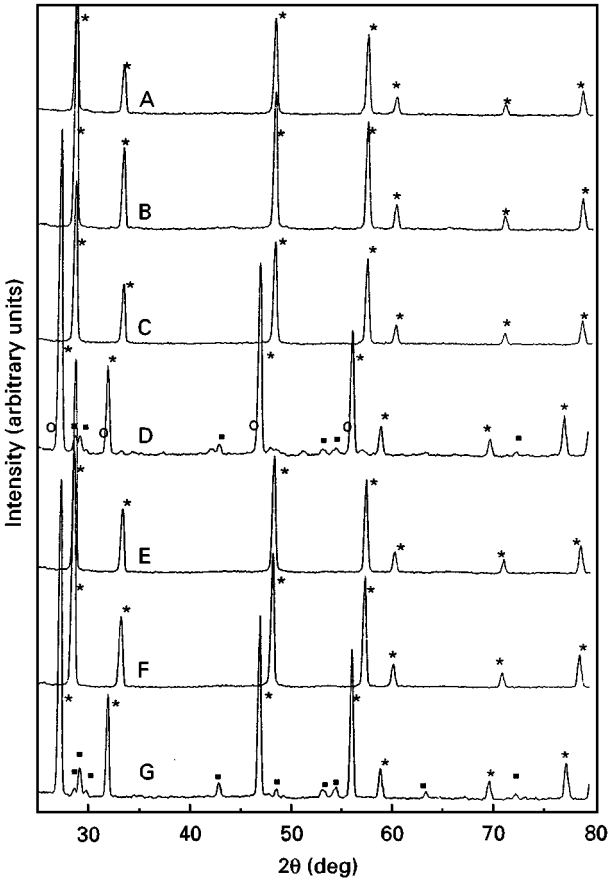

Figure 3 X-ray diffraction patterns of specimens A, B, C, D, E, F and G in the ternary system Y_2O_3–Ta_2O_5–CaO. (*), fluorite; (○), cubic Y_2O_3; (■), monoclinic Ca_2YTaO_6.

was doped with up to 12 mol% CaO. As can be seen in Fig. 2, the X-ray diffraction analysis for specimens Ca8 and Ca12 doped with 8 and 12 mol% CaO, respectively, shows not only the fluorite phase but also other second phases. The other phases were confirmed to be the monoclinic Ca_2YTaO_6 and cubic Y_2O_3 [17]. The monoclinic phase Ca_2YTaO_6, like Ca_2YNbO_6, is a perovskite-type ordered phase (NH_3FeF_6 structure) which forms in the ternary system Y_2O_3–Ta_2O_5 (Nb_2O_5)–CaO and is generally represented as $A_2(B'B'')\,O_6$. In the $A_2(B'B'')\,O_6$ structure, the B site consists of two types of cation B′ and B″ in equimolar ratio, the cation A is divalent and the B-site cations B′ and B″ are trivalent and pentavalent, respectively [17, 18]. The formation of Ca_2YTaO_6 and Y_2O_3 suggests that the solid solution limit of CaO in the fluorite phase $Y_{0.8}Ta_{0.2}O_{1.7}$ is so small at 1650 °C that the excess CaO may react with some of the fluorite phase $Y_{0.8}Ta_{0.2}O_{1.7}$ to produce Ca_2YTaO_6 and Y_2O_3 according to

$$4CaO + Y_8Ta_2O_{17} = 2Ca_2YTaO_6 + 3Y_2O_3 \quad (1)$$

Fig. 3 represents the X-ray diffraction patterns of specimens A, B, C, D, E, F and G, the compositions of which are given in Table II. As shown in Fig. 3, specimens A, B, C, E and F show the X-ray diffraction pattern of the fluorite phase only. However, specimen D, like specimens Ca8 and Ca12 in Fig. 2, shows Ca_2YTaO_6 and Y_2O_3 as the second phases as well as the main fluorite phase.

Specimen Ca4, doped with 4 mol% CaO, shows Y_2O_3 as the second phase and no Ca_2YTaO_6 as shown in Fig. 2; on the other hand, specimen G shows Ca_2YTaO_6 as the second phase and no Y_2O_3 as shown in Fig. 3. As can be seen in Fig. 1, the composition of specimen Ca4 is located between Y_2O_3 and the fluorite phase region, blocking point P, representing the composition Ca_2YTaO_6, from Y_2O_3 so that the perovskite phase Ca_2YTaO_6 cannot be detected by X-ray diffraction analysis. Even if the perovskite phase Ca_2YTaO_6 forms by reaction (1), it may possibly be dissolved in the fluorite phase. In the same way, point G in Fig. 1 is located between the perovskite phase Ca_2YTaO_6 and the fluorite phase blocking Y_2O_3 from Ca_2YTaO_6 so that, even if Y_2O_3 forms by reaction (1), it may possibly be dissolved in the fluorite phase.

Therefore, the shaded region in which points A, B, C, E and F are located as shown in Fig. 1 represents the single-phase region of the fluorite structure. The tangential line to the shaded region drawn from point P, the composition Ca_2YTaO_6, produces the dark region on the left-hand side of the shaded region as shown in Fig. 1. This dark region includes Ca4 and represents the two-phase region of the fluorite and Y_2O_3 phases. The area outside these two regions represents the three phase region of the fluorite,

Y_2O_3 and the monoclinic perovskite Ca_2YTaO_6 phases.

It has been reported that the phase boundary between the region of the fluorite single phase and the two-phase region of the fluorite and Y_2O_3 phases exists at about 80 mol% Y_2O_3 (composition $Y_{0.8}Ta_{0.2}O_{1.7}$) in the binary system Y_2O_3–Ta_2O_5 [16]. The experimental result that CaO has a small solid solution limit with the fluorite phase $Y_{0.8}Ta_{0.2}O_{1.7}$ and produces the perovskite structure $A_2(B'B'')O_6$ can be explained by the fact that the ionic radius of the doped Ca^{2+} ion (0.112 nm; eightfold coordination) [19] is larger than those of the host cations Y^{3+} (0.1019 nm; eightfold coordination) and Ta^{5+} (0.074 nm; eightfold coordination) in the fluorite phase $Y_{0.8}Ta_{0.2}O_{1.7}$.

Fig. 4 shows the X-ray diffraction patterns of specimens Mg4, Mg8, Mg12, Mg16 and Mg20, in which the fluorite phase $Y_{0.8}Ta_{0.2}O_{1.7}$ was doped with 4, 8, 12, 16 and 20 mol% MgO, respectively. It can be seen in Fig. 4 that the fluorite solid solution single phase formed up to 12 mol% MgO. However, the MgO phase appeared as well as the main fluorite solid solution phase when more than 12 mol% MgO was added.

This type of solid solution is considered to be substitutional just like the solid solution of ZrO_2 doped with MgO, CaO or rare-earth oxides. When the addition of MgO exceeded 12 mol%, however, the excess MgO segregated as a second phase and was detected by X-ray diffraction as shown in Fig. 4. This result is in good agreement with the MgO–ZrO_2 system, in which MgO segregates as the second phase because the fluorite phase of ZrO_2 has a limited solid solution range with MgO [20].

Fig. 5 shows the X-ray diffraction patterns of specimens Sr4 and Ba4, in which the $Y_{0.8}Ta_{0.2}O_{1.7}$ fluorite phase was doped with 4 mol% SrO and BaO, respectively. As shown in Fig. 5a and b, two other second phases were observed besides the main fluorite phase for both specimen Sr4 and specimen Ba4. As can be seen in Fig. 5a, one was Y_2O_3 and the other is assumed to be the X-ray diffraction pattern of the cubic Sr_2YTaO_6 for specimen Sr4 because the X-ray diffraction pattern of specimen Sr4 was similar to those of the cubic perovskite type Ba_2YTaO_6 and Sr_2LaNbO_6 [10]. However, the cubic perovskite type Ba_2YTaO_6 phase and cubic Y_2O_3 [21] were observed as the second phases as well as the main fluorite phase $Y_{0.8}Ta_{0.2}O_{1.7}$ for specimen Ba4.

The formation of Sr_2YTaO_6 and Ba_2YTaO_6 together with Y_2O_3 in specimens Sr_4 and Ba_4 means that the solution limits of SrO and BaO with the $Y_{0.8}Ta_{0.2}O_{1.7}$ fluorite phase are so small at 1650 °C that the excess SrO and BaO may react with some of the fluorite phase $Y_{0.8}Ta_{0.2}O_{1.7}$ to produce the cubic

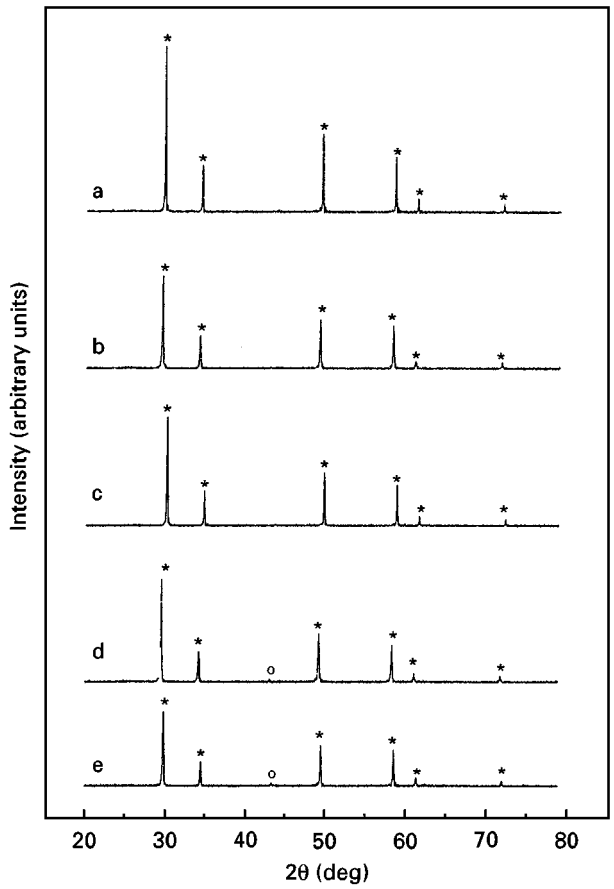

Figure 4 X-ray diffraction patterns of the fluorite $Y_{0.8}Ta_{0.2}O_{1.7}$ specimens doped with 4 mol% MgO (specimen Mg4) (curve a), 8 mol% MgO (specimen Mg8) (curve b), 12 mol% MgO (specimen Mg12) (curve c) 16 mol% MgO (specimen Mg16) (curve d) and 20 mol% MgO (specimen Mg20) (curve e). (*), fluorite; (○), MgO.

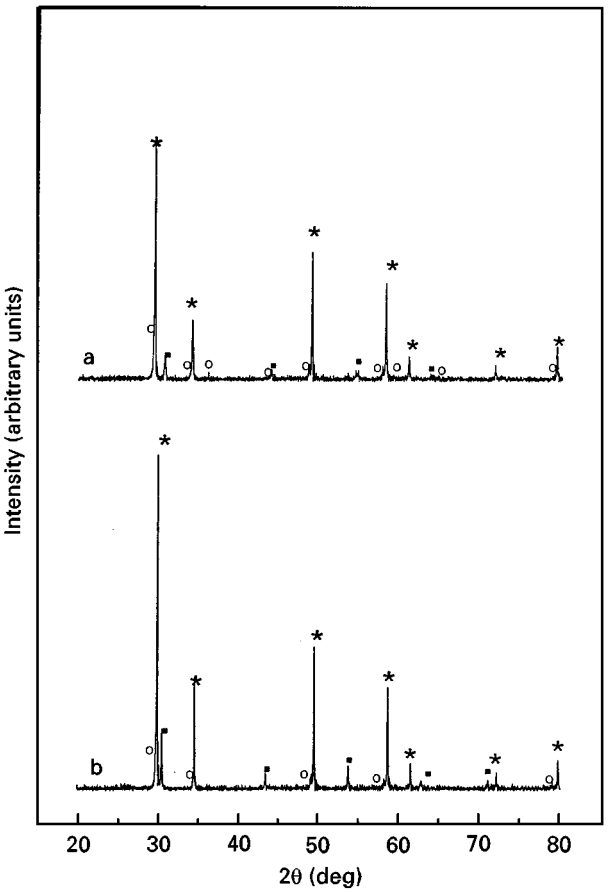

Figure 5 X-ray diffraction patterns of the fluorite $Y_{0.8}Ta_{0.2}O_{1.7}$ specimens doped with 4 mol% SrO (specimen Sr4) (curve a) and 4 mol% BaO (specimen Ba4) (curve b). (*), fluorite; (○), cubic Y_2O_3; (■), cubic Sr_2YTaO_6 for curve a and cubic Ba_2YTaO_6 for curve b.

$A_2(B'B'')\,O_6$ phase of Sr_2YTaO_6 and Ba_2YTaO_6 and the other cubic phase Y_2O_3 by

$$4SrO + Y_8Ta_2O_{17} = 2Sr_2YTaO_6 + 3Y_2O_3 \quad (2)$$

$$4BaO + Y_8Ta_2O_{17} = 2Ba_2YTaO_6 + 3Y_2O_3 \quad (3)$$

This is because the ionic radii of the doped Ba^{2+} ion (0.142 nm; eightfold coordination) and the Sr^{2+} ion (0.126 nm; eightfold coordination) are larger than that of the Ca^{2+} ion (0.112 nm; eightfold coordination). Even in the BaO–ZrO_2 and SrO–ZrO_2 systems which are known to form the fluorite phase easily, the fluorite phase was reported to form at above 2200 °C and less than about 5 mol% [22, 23].

Fig. 6 shows the regions of formation of the fluorite phase and other related phases according to the amount of the doped alkaline-earth oxides and the sizes of ionic radii of the dopants compared with those of the host cations. The sizes of ionic radii of cations which construct $Y_{0.8}Ta_{0.2}O_{1.7}$ fluorite structure are represented together with the mean values of the cations of the oxides along the abscissa for comparison. It can be seen in Fig. 6 that the fluorite phase could be doped with larger amounts of MgO than other alkaline-earth oxides such as CaO, BaO and SrO because the radius of the Mg^{2+} ion is smaller than the mean value for the host cations Y^{3+} and Ta^{5+} of the fluorite phase to form the fluorite phase solid solution. On the other hand, the fluorite phase could be doped with less CaO than MgO because the radius of Ca^{2+} is a little larger than that of the Y^{3+} ion. The Sr^{2+} and Ba^{2+} ions, whose ionic radii are much larger than those of the Ca^{2+} ion as well as the Y^{3+} ion, could not be used at all to form the fluorite solid solution.

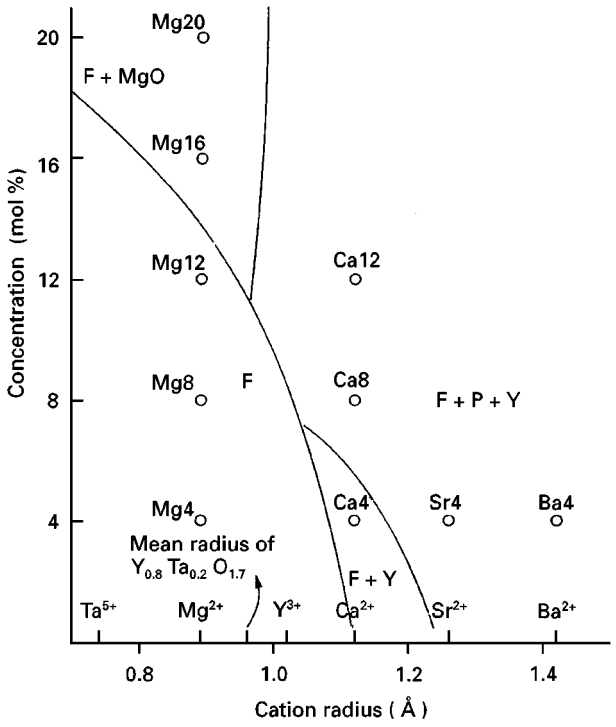

Figure 6 Phase relations at 1650 °C in the system $Y_{0.8}Ta_{0.2}O_{1.7}$–MO (M = Mg, Ca, Sr or Ba). F, fluorite phase; P, perovskite; Y, Y_2O_3

Unlike the system $Y_{0.8}Ta_{0.2}O_{1.7}$–alkaline-earth oxide, ZrO_2 easily produces solid solutions with various divalent or trivalent cationic oxides. ZrO_2 easily forms the cubic fluorite solid solution not only with Mg^{2+} and Sc^{3+} ions whose ionic radii are larger than that of the Zr^{4+} ion but also with Ca^{2+} and Y^{3+} ions whose radii are much larger than that of the Zr^{4+} ion. The Sc_2O_3–ZrO_2 system forms the fluorite solid solution in the range 16–33 mol% Sc_2O_3, the MgO–ZrO_2 system in the range 10–30 mol% MgO, the CaO–ZrO_2 system in the range 10–20 mol% CaO and the Y_2O_3–ZrO_2 system in the range 9–55 mol% Y_2O_3 [4].

Therefore, ZrO_2 forms the cubic fluorite solid solution with even larger cations than the Zr^{4+} ion because the radius of the Zr^{4+} ion is small; however, the $Y_{0.8}Ta_{0.2}O_{1.7}$ fluorite phase forms the fluorite solid solution not with larger cations than the Y^{3+} ion but with smaller cations than Y^{3+} because the Y^{3+} ion of the constituent is large enough. This suggestion is supported by the fact that MgO could be used to dope the fluorite phase in as high a concentration as other alkaline-earth oxides.

Consequently, it is assumed that the formation of the fluorite phase in the system of Y_2O_3–Ta_2O_5–MO (M = Mg, Ca, Sr or Ba), including the system $Y_{0.8}Ta_{0.2}O_{1.7}$–MO, is greatly influenced by the size of the cationic radus of the alkaline-earth oxide dopant.

4. Conclusions

The formation regions of the fluorite phase and other related phases in the system Y_2O_3–Ta_2O_5–MO (M = Mg, Ca, Sr or Ba) at 1650 °C have been studied using the X-ray diffraction method. The results obtained are summarized as follows.

1. When the fluorite phase $Y_{0.8}Ta_{0.2}O_{1.7}$ was doped with up to 12 mol% MgO, the fluorite single phase was obtained. However, MgO segregated when the fluorite phase was doped with more than 16 mol% MgO.

2. When the fluorite phase $Y_{0.8}Ta_{0.2}O_{1.7}$ was doped with 8 and 12 mol% CaO, the monoclinic perovskite phase Ca_2YTaO_6 and cubic phase Y_2O_3 were produced as well as the main fluorite phase by the reaction of the excess CaO with some of the fluorite phase because CaO has a limited solid solution range with the fluorite phase. This is because the ionic radius of the doped Ca^{2+} ion is larger than the mean radius of the host Y^{3+} and Ta^{5+} ions which construct the fluorite phase. However, when the fluorite phase was doped with 4 mol% CaO, only Y_2O_3 was detected as the second phase. This is because the composition containing 4 mol% CaO is located between Y_2O_3 and the fluorite phase in the phase diagram of the system Y_2O_3–Ta_2O_5–CaO so that the perovskite phase Ca_2YTaO_6 cannot exist in that region. Even though Ca_2YTaO_6 forms a little in that region, it may be dissolved into the fluorite phase. Y_2O_3 cannot be produced in the composition region between Ca_2YTaO_6 and the fluorite phase for a similar reason to the case of the composition containing 4 mol% CaO.

3. The oxides SrO and BaO have little solid solution range with the fluorite phase so that the specimens doped with most SrO and BaO react with the fluorite phase to produce Sr_2YTaO_6–Y_2O_3 and Ba_2YTaO_6–Y_2O_3, respectively, as the second phases. This is because the ionic radius of the doped Sr^{2+} or Ba^{2+} ion is larger than the mean radius of the host cations Y^{3+} and Ta^{5+}.

4. The formation of the fluorite phase and other related phases in the system $Y_{0.8}Ta_{0.2}O_{1.7}$–alkaline earth oxide is greatly influenced by the size of the cation of the alkaline-earth oxide dopant.

Acknowledgement

Financial support for this work from the Korean Ministry of Education Research Fund for Advanced Materials in 1996 is gratefully acknowledged.

References

1. N. Q. MINH, *J. Amer. Ceram. Soc.* 76 (1993) 563.
2. E. M. LOGOTHETIS, in "Advances in Ceramics", Vol. 3, "Science and Technology of Zirconia", edited by A. H. Heuer and L. W. Hobbs (American Ceramic Society, Columbus, Ohio, 1981) pp. 388–405.
3. F. S. GALASSO, in "Structure and properties of inorganic solids", International Series of Monographs in Solid State Physics, Vol. 7, edited by N. Kurti and R. Smoruchowski (Pergamon Press, Oxford, 1970) pp. 82–119.
4. T. H. ETSELL and S. N. FLENGAS, *Chem. Rev.* **70** (1970) 339.
5. A. KVIST, in "Physics of Electrolytes", Vol. 1, "Transport process in solid electrolytes and in electrodes", edited by J. Hladik (Academic Press, New York, 1972) pp. 319–346.
6. C. WAGNER, *Naturwissenschaften*, **31** (1943) 265.
7. C. B. CHOUNDRY and E. C. SUBBARAO, in "Fast ion transport in solids", edited by P. Vashishta, J. Mundy and G. Shenoy (Elsevier North-Holland, New York, 1979) pp. 665–668.
8. D. J. KIM and T. Y. TIEN, *J. Amer. Ceram. Soc.*, **74** (1991) 3061.
9. C. ZHENG and A. R. WEST, *Brit. Ceram. Tran. J.* **89** (1990) 138.
10. G. W. JORDAN, M. G. McTAGGART and M. F. BERARD, *J. Solid State Chem.* **56** (1985) 360.
11. D. MICHEL and M. P. JORBA, *J. Amer. Ceram. Soc.* **65** (1982) C-135.
12. Z. HUANG, D. YAN, T. TIEN and I. CHEN, *Mater. Lett.* **11** (1991) 286.
13. N. MIZUTANI, Y. TAJIMA and M. KATO, *J. Amer. Ceram. Soc.* **59** (1976) 168.
14. G. V. SHAMRAI, A. V. ZAGORODNYUK, R. L. MAGUNOV and A. P. ZHINOVA, *Russ. J. Inorg. Chem.*, **29** (1984) 1811.
15. Y. YOKOGAWA, N. ISHIZAWA, S. SOMIYA and M. YOSHIMURA, *J. Amer. Ceram. Soc.* **74** (1991) 2073.
16. Y. YOKOGAWA and M. YOSHIMURA, *ibid.* **74** (1991) 2077.
17. F. S. GALASSO, in: "Structure and properties of inorganic solids", International Series of Monographs in Solid State Physics, Vol. 7, edited by N. Kurti and R. Smoruchouski (Pergamon Press, Oxford, 1970) pp. 162–210.
18. F. GALASSO, G. LAYDEN and D. FLINCHBAUGH, *J. Chem. Phys.* **44** (1966) 2703.
19. R. D. SHANNON, *Acta Crystallogr. A* **32** (1976) 751.
20. P. DURAN, J. M. RODRIGUEZ and P. RECIO, *J. Mater. Sci.* **26** (1991) 467.
21. Joint Committee on Powder Diffraction Standards, "Powder diffraction file" (International Center for Diffraction Standards, Swarthmore, PA, 1979), Card 19–147.
22. A. V. SHEVCHENKO, L. M. LOPATO, G. F. GERASIMYUK and Z. A. ZAITSEVA, *Inorg. Mater.* **23** (1987) 1322.
23. T. NOGUCHI, T. OKUBO and O. YONEMOCHI, *J. Amer. Ceram. Soc.* **52** (1969) 181.

Received 9 June 1997
and accepted 5 February 1998